Numerical investigation of mining-induced strata disturbances using a discontinuous deformation and displacement coupling method

To cite this article: Xindang Yang *et al* 2021 *IOP Conf. Ser.: Earth Environ. Sci.* **861** 032075

Numerical investigation of mining-induced strata disturbances using a discontinuous deformation and displacement coupling method

Xindang Yang, Zhengzhao Liang*, Bin Gong

State Key Laboratory of Coastal and Offshore Engineering, Dalian University of Technology, Dalian, 116024, China

*Corresponding author, Email: liangzz@dlut.edu.cn, ORCID: 0000-0002-8634-4458

Abstract. Strata movement and ground subsidence caused by mining have a significant influence on the safety and stability of the goaf. By taking the mesoscopic heterogeneity of rock masses into account, the discontinuous deformation and displacement (DDD) method was applied to simulate the whole failure process of overlying strata after coal mining under different advancing distances of the working face. The results show that key strata would not be broken when the working face was advanced by 30 m. When the advancing distance increased to 50 m, the first key stratum was broken; when it went up to 70 m, both the first and the second key strata were broken and collapsed successively. Moreover, the bed separation of strata had become particularly obvious and a three-zone phenomenon—including collapsed zone, fractured zone, and continuous deformation zone—presented throughout the whole rock mass when the distance rose to 90 m. As the working face is advanced by increasing distances, there are increases in the ranges of deformation, disturbance, and damage in the overlying strata, as well as surface settlement. Meanwhile, the gradual collapse process of the strata is further analyzed in terms of the background-stress evolution; i.e., stress accumulation, stress shadow, and stress transference. Furthermore, it has been proven that the DDD method is an effective approach to reproduce the whole process of strata collapse and macro instability from small deformation, crack initiation, and propagation to block translation, rotation, and contact, which is crucial for predicting strata movement and surface subsidence.

1. Introduction

Coal is a unique nonrenewable energy resource for industrial production and economic development. Under the excavation disturbance of coal mining, the overlying strata of a goaf may deform, fracture, and collapse, which could cause ground deformation and even a large area of surface subsidence, potentially bringing huge losses of life and property [1, 2]. Therefore, the overlying strata movement and surface subsidence caused by coal mining has always been a challenging and significant topic in rock mechanics. Generally, there are four main methods to study strata movement and mining subsidence: theoretical analysis, in situ monitoring, laboratory testing, and numerical modeling. However, theoretical analysis usually presupposes that the rock material is homogeneous and, thus, simplifies many difficulties and puts limits on practical applications. Additionally, due to the limited monitoring points, it is impossible to accurately grasp the entire stress and deformation fields of an engineering area. Also, physical testing is restricted by the effect of small sample sizes, instrument

performance, and high cost. In contrast, numerical simulation has been widely used to model the mechanical behaviors of rocks because of its convenience, efficiency, and reliability.

At present, the finite element method (FEM), finite difference method, and other continuum-mechanics–based numerical methods encounter many mathematical problems such as large mesh deformation and fracture behavior, which make calculations impossible [3, 4]. Therefore, Tang [5] developed the FEM-based rock fracture process analysis (RFPA) method to overcome the shortcomings of conventional FEM and model the progressive failure behaviors of discontinuous media. However, RFPA cannot handle contact-sliding between newly formed rock blocks, and therefore, cannot simulate the whole process of strata deformation, failure, and collapse caused by mining. Conversely, to consider the discontinuity of an engineering rock mass, some researchers have attempted to develop a discontinuous medium method to simulate rock-related issues. The discrete element method (DEM) [6] and the discontinuous deformation analysis (DDA) method [7] are representative of this work. Although discontinuous medium methods can calculate discontinuous deformation and contacts of blocks for the exploration of strata movement behavior, they suffer many typical difficulties. For example, the topological structure has a significant influence on computed results. Cracks cannot form in blocks, the stress and strain fields within blocks are coarse, and they consume many computing time with low efficiency. Therefore, a more effective analysis method is needed to comprehensively study such problems. To combine the advantages of continuous medium methods and discontinuous medium methods to analyze this kind of problem, Tang et al. [8] and Gong et al. [9] have proposed the discontinuous deformation and displacement (DDD) method that inherits the advantages of both RFPA and DDA to model crack growth as well as mechanical interactions including contacting, detaching, and sliding.

In this work, the deformation and failure characteristics of the strata were simulated by DDD, and the strata movement behavior under different advancing distances in a single working face was further discussed from the aspects of the displacement field and stress field.

2. The basic principles of the DDD method

2.1. Constitutive model of mesoelements

To consider the significant influence of the mesoscopic heterogeneity of rock materials on the macro nonlinearity, the Weibull distribution [10] is adopted to realize the nonuniform distribution of material parameters. The probability density function can be expressed as follows:

$$\emptyset(\varphi) = \frac{m}{\varphi_0} \cdot (\frac{\varphi}{\varphi_0})^{m-1} \cdot e^{-(\frac{\varphi}{\varphi_0})_m} \quad (1)$$

where $\boldsymbol{\varphi}$ is a mechanical parameter of mesoelements; $\boldsymbol{\varphi_0}$ represents the average value of the corresponding mechanical parameter, $\boldsymbol{\varphi}$; and $\boldsymbol{m}$ is the homogeneity coefficient; the greater the value of $\boldsymbol{m}$ is, the more uniform the material property is.

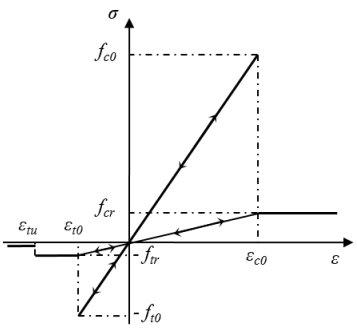

Figure 1. Stress-strain relationship of an element under uniaxial compression and tension.

The mesoelements that are used to establish numerical models are initially considered to be linear elastic. When the stress state of an element reaches a specific strength criteria, the element begins to

damage. The elastic modulus of the damaged element will decrease with the damage evolution, and the evolution is described as follows:

$$E = (1 - D)E_0 \tag{2}$$

where $\boldsymbol{E_0}$ and $\boldsymbol{E}$ are the initial and damaged elastic moduli, respectively; and $\boldsymbol{D}$ is the damage variable. The maximum tensile stress/strain criterion and Mohr–Coulomb criterion are adopted. Taking the constitutive relation of an element under uniaxial stress as an example (Figure 1), the expression of the damage variable $\boldsymbol{D}$ under different stress states can be determined. When the stress/strain state of a particular element reaches the maximum tensile stress/strain criterion, the element will be damaged in tension mode. Similarly, when the stress/strain states of the mesoelements under uniaxial compression satisfy the Mohr–Coulomb criterion, shear damage occurs.

2.2. Global equilibrium equation

The global equilibrium equation can be obtained by deriving the potential energy to the displacement vector and taking the extreme value according to the principle of minimum potential energy, shown as follows:

$$\begin{bmatrix} K_{11} & K_{12} & \cdots & K_{1m} \\ K_{21} & K_{22} & \cdots & K_{2m} \\ \vdots & \vdots & & \vdots \\ K_{i1} & K_{i2} & \cdots & K_{im} \\ \vdots & \vdots & & \vdots \\ K_{m1} & K_{m2} & \cdots & K_{mm} \end{bmatrix} \begin{bmatrix} d_1 \\ d_2 \\ \vdots \\ d_i \\ \vdots \\ d_m \end{bmatrix} \begin{bmatrix} F_1 \\ F_2 \\ \vdots \\ F_i \\ \vdots \\ F_m \end{bmatrix} \tag{3}$$

where $\boldsymbol{K_{ij}}$ is a 2 × 2 submatrix, $\boldsymbol{F_i}$ is the external loading submatrix, and $\boldsymbol{d_i}$ is the displacement submatrix of node $\boldsymbol{i}$, which contains two components $\{u_i \quad v_i\}^T$. $\boldsymbol{u_i}$ and $\boldsymbol{v_i}$ are the translations of node $\boldsymbol{i}$ along the $\boldsymbol{x}$- and $\boldsymbol{y}$-axes, respectively. According to the derivation, if $\boldsymbol{w_i}$ represents any component of ($\boldsymbol{u_i}$, $\boldsymbol{v_i}$), then the displacement at point ($\boldsymbol{x}$, $\boldsymbol{y}$) within element $\boldsymbol{p}$ can be calculated by the following equations:

$$w_{(x,y)} = \frac{1}{2\Delta}(1 \quad x \quad y) \begin{bmatrix} x_j y_m - x_m y_j & x_m y_i - x_i y_m & x_i y_j - x_j y_i \\ y_j - y_m & y_m - y_i & y_i - y_j \\ x_m - x_j & x_i - x_m & x_j - x_i \end{bmatrix} \begin{Bmatrix} w_i \\ w_j \\ w_m \end{Bmatrix} \tag{4}$$

The partial potential energy can be added to the global equilibrium equation, including:

(1) The strain energy Π_e applied by the initial stress and elastic stress of an element $\boldsymbol{i}$ is defined as:

$$\Pi_e^i = \frac{1}{2}\iint \varepsilon_i^T \sigma_i \, \boldsymbol{dx\,dy} + \iint \varepsilon_i^T \sigma_i^0 \, \boldsymbol{dx\,dy} \tag{5}$$

where $\boldsymbol{\sigma_i}$ and $\boldsymbol{\varepsilon_i}$ are the stress and strain of the element $\boldsymbol{i}$, respectively, and $\boldsymbol{\sigma_i^0}$ is the corresponding initial stress.

(2) The potential energy of the point loading $\boldsymbol{p_i} = \{p_x^i \quad p_y^i\}^T$ is:

$$\Pi_p^i = -(p_x^i u_i + p_y^i v_i) \tag{6}$$

where $\boldsymbol{p_x^i}$ and $\boldsymbol{p_y^i}$ are the two components of $\boldsymbol{p_i}$ along the $\boldsymbol{x}$- and $\boldsymbol{y}$-axes, respectively.

(3) The potential energy of the displacement constraints on the node $\boldsymbol{i}$ is:

$$\Pi_c^i = \frac{k}{2}d^2 \tag{7}$$

where $\boldsymbol{k}$ is stiffness of the constraint spring and $\boldsymbol{d}$ is the a presetting boundary displacement.

(4) The potential energy of the constant body force $\boldsymbol{b_i} = \{b_x^i \quad b_y^i\}^T$ is:

$$\Pi_b^i = -\iint (b_x^i u + b_y^i v) \, \boldsymbol{dx\,dy} \tag{8}$$

where $\boldsymbol{b_x^i}$ and $\boldsymbol{b_y^i}$ are the two components of $\boldsymbol{b_i}$ along the $\boldsymbol{x}$- and $\boldsymbol{y}$-axes, respectively.

(5) The potential energy of the contact springs is:

$$\Pi_k = \frac{k_n}{2}d_n^2 + \frac{k_t}{2}d_t^2 \tag{9}$$

where $\boldsymbol{k_n}$ and $\boldsymbol{k_t}$ are the normal stiffness and shear spring stiffness, respectively; and $\boldsymbol{d_n}$ and $\boldsymbol{d_t}$ are the normal spring deformation and shear spring deformation, respectively.

3. The influence of advancing distance of the working face on strata movement

3.1 Establishment of numerical model

A representative numerical model is established as shown in Figure 2. The length and height of the whole model are 150 m and 70 m, respectively. The top surface of the model is free, the bottom is constrained along with the vertical and horizontal directions simultaneously, and the left and right boundaries are constrained along the horizontal direction. The numerical model consists of 93,400 finite elements, and the physical and mechanical parameters for different rock formations are listed in Table 1. Two thick and hard rock layers can be regarded as the key strata. The advancing distances of the working face are set to be 30 m, 50 m, 70 m, and 90 m, respectively. In other words, except for the advancing distance, the rock parameters and boundaries will remain unchanged under different simulations.

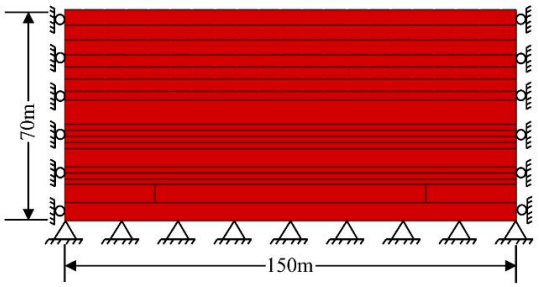

Figure 2. Numerical model for different advancing distances of the working face.

Table 1. Physical and mechanical parameters for different rock formations.

Vertical range (m)	Density (kg/m^3)	Elastic modulus (GPa)	Cohesion (MPa)	Fiction angle (°)	Tensile strength (Mpa)	Poisson's ratio
55~70	2600	20	28	30	7	0.25
40~55	2600	10	14	30	3.5	0.25
32~40	2600	16	24	30	5	0.25
24~32	2600	9	12	30	2.5	0.25
18~24	2600	12	20	30	3	0.25
12~18	2600	8	10	30	1.5	0.25
6~12	2600	10	Max	30	Max	0.25
0~6	2600	40	Max	30	Max	0.25

3.2 Movement of overlying strata

Figure 3 shows the simulated development process of strata movement when the advancing distance of the working face is 30 m, from which we can see that the three strata above the goaf begin to move downward after excavation, but the first key stratum is stable. When the calculation is carried out to 2020 steps, the roof falls further down and gets broken obviously. After 3652 steps, the three immediate roofs fall onto the floor and are seriously damaged. Meanwhile, the first key stratum remains undamaged.

The development process of strata movement when the working face is advanced to 50 m is depicted in Figure 4. After 4105 steps, the cracks distributed in the first key stratum further propagate, and the vertical displacement of the immediate roof increases. Meanwhile, a collapsing trend occurs.

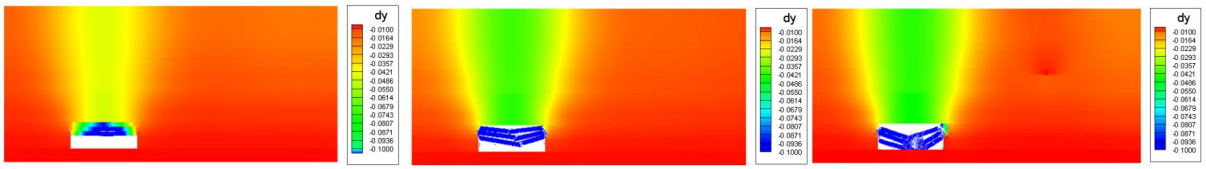

(a) step 516 **(b) step 2020** **(c) step 3652**

Figure 3. Strata movement indicated by vertical displacement contours when the advancing distance is 30 m.

When the calculation is carried out to 7051 steps, many small blocks are formed in the three immediate roofs. Moreover, the first key stratum is further broken and the subsidence deformation of overlying strata becomes more obvious. After 11022 steps, the rock strata are fully collapsed and fall down on the floor. In the meantime, an obvious difference from the case of 30 m advancing distance is that the first key stratum has failed, but the second key stratum is stable with several small cracks.

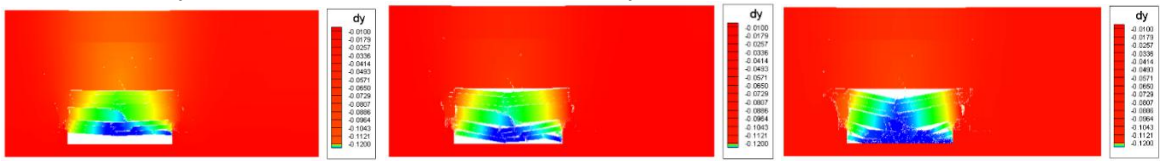

(a) step 4105 **(b) step 7051** **(c) step 11022**

Figure 4. Strata movement indicated by vertical displacement contours when the advancing distance is 50 m.

Figure 5 demonstrates the subsidence process of rock strata when the advancing distance of the working face is 70 m, from which we can see that the fractures occurring at both ends of the excavation area extend higher than in the cases of 30 m and 50 m advancing distances. Both the first key stratum and the second key stratum are damaged, leading to the failure of the entire overburden rock mass.

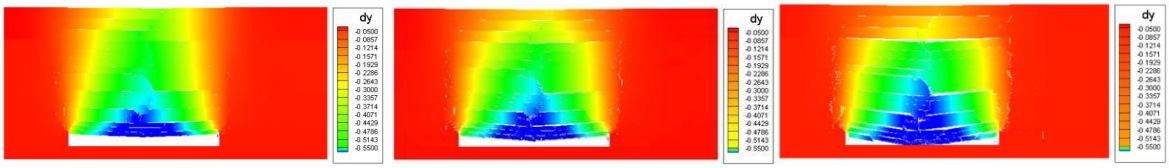

(a) step 3025 **(b) step 5023** **(c) step 8010**

Figure 5. Strata movement indicated by vertical displacement contours when the advancing distance is 70 m.

Figure 6 indicates that the detailed fracture characteristics are much more complicated than the conventional three-zone division [11]. When the working face is advanced to 90 m, the collapsed zone including the three immediate roofs, the bed separation zone including the rock layers between the two key strata, and the near-ground rupture zone including the rock layers under the ground surface are observed. After the excavation of the coal seam at step 3017, the immediate roofs gradually and irregularly collapse due to the heterogeneity of rock masses, forming a collapsed zone. Then at step 5007, the above overlying strata develop numerous cracks, bending fractures, sinkage, and layer separation. The bed separation is adjacent to the collapsed zone. When the calculation is performed to 7500 steps, the rock strata in the lower part of the near-ground rupture zone break into many blocks, and the fracture degree of the rock strata gradually decreases from bottom to top. Although this zone between the surface and the second key stratum is a bending subsidence zone, the strata in this area are not continuous because of the existence of the cracks. Compared with the other three cases, the

overlying strata are more extensively destroyed, and the surface is affected by the movement of the lower strata, resulting in greater subsidence. Additionally, by comparing the final failure patterns of the four cases, it is found that with the advancing distance of the working face, the damage degree, fracture range, and ground subsidence increase correspondingly.

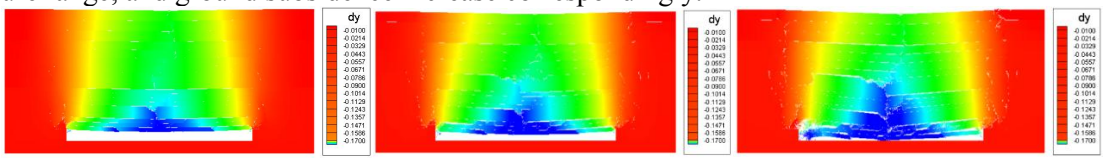

(a) step 3017 **(b) step 5007** **(c) step 7500**

Figure 6. Strata movement indicated by vertical displacement contours when the advancing distance is 90 m.

Figure 7 is the maximum principal stress diagram of the rock strata under four different mining distances. With the increase of distance, stress concentration occurs at both ends of the excavation area and at the crack tips. The deformation development range is also expanded. Different-sized stress concentrations occurred between adjacent rock layers, especially in the key strata. When the key strata are damaged, the stress and energy are released.

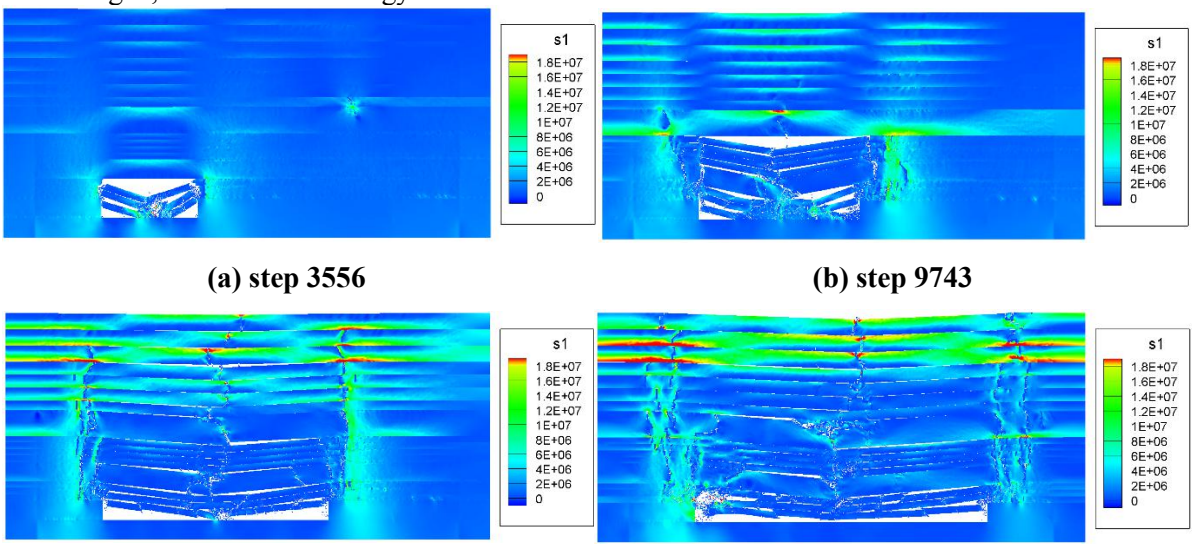

(a) step 3556 **(b) step 9743**

(c) step 7038 **(d) step 6987**

Figure 7. Strata movement indicated by maximum principal stress contours when the advancing distance is 90 m.

4. Conclusions

In this study, the deformation and failure characteristics of strata are modeled by the DDD method by considering that brittle fractures are bred at the small deformation stage and the macroscopic nonlinearity of rock masses originates from their mesoscopic heterogeneity. The main conclusions are as follows: The DDD method is used to simulate and analyze the influence of different advancing distances of the working face on overlying strata movement. When the advancing distance is small, the three immediate roofs get damaged seriously and the first key stratum controls the local instability. With the increase of advancing distance, the bed separation phenomenon between two adjacent strata is particularly clear due to discordant deformation. When the advancing distance is large, the collapsed zone including the three immediate roofs, the bed separation zone including the rock layers between the two key strata, and the near-ground rupture zone including the rock layers under the ground

surface are observed. To conclude, DDD can reflect actual fracture characteristics and effectively explain the law of strata fracture and movement, which can be used in studying strata movement–related problems.

Acknowledgments
This work is financially supported by the National Natural Science Foundation of China (Grant No. 41977219) and the China Postdoctoral Science Foundation (Grant No. 2020M680950).

References

[1] E. F. Salmi, M. Nazem, and M. Karakus, "The effect of rock mass gradual deterioration on the mechanism of post-mining subsidence over shallow abandoned coal mines," *International Journal of Rock Mechanics and Mining Sciences,* vol. 91, pp. 59-71, 2017.
[2] Y. Sun, J. Zuo, M. Karakus, and J. Wang, "Investigation of movement and damage of integral overburden during shallow coal seam mining," *International Journal of Rock Mechanics and Mining Sciences,* vol. 117, pp. 63-75, 2019.
[3] S. S. Bahrainian and A. D. Dezfuli, "A geometry-based adaptive unstructured grid generation algorithm for complex geological media," *Computers & Geosciences,* vol. 68, pp. 31-37, 2014.
[4] B. Vazhbakht and A. M. Zsaki, "A finite element mesh optimization method incorporating geologic features for stress analysis of underground excavations," *International Journal of Rock Mechanics and Mining Sciences,* vol. 59, pp. 111-119, 2013.
[5] C. Tang, "Numerical simulation of progressive rock failure and associated seismicity," *International Journal of Rock Mechanics Mining Sciences,* vol. 34, no. 2, pp. 249-261, 1997.
[6] P. A. Cundall and O. D. L. Strack, "A discrete numerical model for granular assemblies," *Géotechnique,* vol. 30, no. 3, pp. 331-336, 2008.
[7] G. Shi, "Discontinuous Deformation Analysis: A New Numerical Model for the Statics and Dynamics of Deformable Block Structures," *Engineering Computations,* vol. 9, no. 2, pp. 157-168, 1992.
[8] C. Tang, S. Tang, B. Gong, and H. Bai, "Discontinuous deformation and displacement analysis: From continuous to discontinuous," *Science China Technological Sciences,* vol. 58, no. 009, pp. 1567-1574, 2015.
[9] B. Gong, C. a. Tang, S. Wang, H. Bai, and Y. Li, "Simulation of the nonlinear mechanical behaviors of jointed rock masses based on the improved discontinuous deformation and displacement method," *International Journal of Rock Mechanics and Mining Sciences,* vol. 122, 2019.
[10] W. Weibull, "Wide applicability," *Journal of Applied Mechanics,* vol. 18, pp. 293-297, 1951.
[11] F. Gao, D. Stead, and J. Coggan, "Evaluation of coal longwall caving characteristics using an innovative UDEC Trigon approach," *Computers and Geotechnics,* vol. 55, pp. 448-460, 2014.

Appendix 1

A table listing all parameters and symbols used in equations and formulations throughout the paper is included in this appendix.

Lists of symbols	Explanations
$\boldsymbol{\varphi}$	Mechanical parameter of mesoelements
$\boldsymbol{\varphi_0}$	average value of $\boldsymbol{\varphi}$
$\boldsymbol{m}$	Homogeneity coefficient
$\boldsymbol{E_0}$	Initial elastic modulus
$\boldsymbol{E}$	Damaged elastic modulus
$\boldsymbol{D}$	Damage variable
$\boldsymbol{F_i}$	External loading submatrix
$\boldsymbol{d_i}$	Displacement submatrix of Node $\boldsymbol{i}$
$\boldsymbol{u_i}$	Translation of Node $\boldsymbol{i}$ along the $\boldsymbol{x}$ axe

v_i	Translation of Node i along the y axe
w_i	Any component of (u_i, v_i)
σ_i	Stress of the element i
ε_i	Strain of the element i
σ_i^0	Initial stress of the element i
p_i	Potential energy of the point loading
k	Stiffness of the constraint spring
d	Presetting boundary displacement
b_i	Potential energy of the constant body force
k_n	Normal stiffness
k_t	Shear springs stiffness
d_n	Normal spring deformation
d_t	Shear spring deformation